

Influence of the nucleon spectral function in photon and electron induced reactions on nuclei

J. Lehr and U. Mosel

*Institut für Theoretische Physik, Universität Giessen
D-35392 Giessen, Germany*

(Dated: October 29, 2018)

We study the influence of the nucleon spectral function on η photo- and electroproduction on nuclei. Besides kinematical effects due to groundstate correlations, also a modification of the $S_{11}(1535)$ decay width is taken into account, which is caused by the possible decay into nucleons with mass smaller than the pole mass in the medium. Hence, resonances with masses below the free $N\eta$ threshold can contribute to η production.

PACS numbers: 25.30.Rw, 25.20.Lj

I. INTRODUCTION

Nucleons inside nuclei are commonly described in terms of quasi particles with an effective mass connected to the mean-field potential. However, it is also known that such strongly interacting particles obtain a finite width [1] from processes that correspond in lowest order (beyond the mean-field approximation) to collision reactions. The so-called collisional broadening is therefore a feature that should be accounted for in nuclear reactions where the nucleons frequently collide with each other or with other particles. The nucleons in the nuclear groundstate are subject to a broadening due to short-range correlations (see e.g. [2, 3, 4, 5]). In inclusive reactions such as electron scattering off nuclei these effects have been taken into account and proven to have influence (e.g. [6]). In [7, 8] photon induced $K^+\Lambda$ production and proton induced production of heavy mesons K^+, ρ, ω, ϕ on carbon has been studied within the framework of folding models showing also an influence in more exclusive reactions. In the energy regime where nucleon resonances play an important role there is another modification that should be taken into account: In the vacuum, it is known that the decay width of resonances into channels with unstable mesons (e.g. $R \rightarrow N\rho$) is strongly influenced by the meson spectral function. If the rho meson was a stable particle with a mass of 770 MeV, a $D_{13}(1520)$ resonance with a mass of 1.524 GeV could not decay into $N\rho$. However, the branching ratio into this channel is in the range of 15-25% [9]. Therefore, also the decay width of the nucleon resonances into channels with nucleons should change when the nucleon spectral function deviates from a delta function in the medium.

In the framework of transport models, theoretical concepts for the offshell propagation of nucleons have been developed [10, 11, 12], which was a prerequisite for the treatment of offshell nucleons in heavy-ion reactions. We are, therefore, now in a position to be able to combine the aspects of the groundstate correlations and the nucleon spectral function in the FSI as well as the propagation to study more exclusive reactions with electromagnetic probes. In this work, we consider η photo- and electroproduction on nuclei ($T = 0$) in the second resonance region and study the influence of the nucleon spectral function. For these energies, this channel is particularly interesting, because of the strong connection between the η meson and the $S_{11}(1535)$ resonance. In particular we will focus on the sensitivity of such reactions on the groundstate correlations and the modification of the $S_{11}(1535)$ decay width. For our calculations on nuclei we use a semi-classical BUU transport model, which we already used for the calculation of these processes using the onshell approximation for the nucleons [13, 14].

We start in Sec. II with a discussion of the nucleon spectral function used in our calculations. In Sec. III we describe how the decay widths are modified by the nucleon spectral function in the medium, followed by some details about the the calculation of the cross sections on nuclei and the BUU model in Sec. IV and V. In Sec. VI we show our results on η photo- and electroproduction on calcium.

II. THE NUCLEON SPECTRAL FUNCTION

The influence of the nucleon spectral function is twofold: On the one hand, there are correlations between the nucleons in the nuclear groundstate leading to a finite width. The nucleon spectral function in nuclear matter was calculated in [4, 5] using transport theoretical methods. The width was obtained by calculating collision widths. There it was found that for a description of the spectral function properties the knowledge of the overall strength of the nucleon interaction is already sufficient. Determining this parameter from more sophisticated many-body models [2], both momentum cuts of the spectral function and the momentum distribution are in very good agreement with such approaches. We have performed the same calculations for different densities. Using local density approximation,

we were then able to apply our nucleon spectral function also to the groundstate of finite nuclei. A similar procedure was used in [15] to obtain the momentum distribution in finite nuclei. In Fig. 1 we show the mass and momentum spectra in a calcium nucleus, determined by the spectral function. It is seen that the mass spectrum shows a strong asymmetry with respect to the still dominating onshell peak; most nucleons off the mass shell have masses $\mu < m_N$. This can be easily understood if we consider for simplicity nuclear matter. In the groundstate all states with energy smaller than the Fermi energy E_F are occupied. The nucleons with pole mass m_N obey the condition $E = \sqrt{m_N^2 + p^2}$. The region in the (E, p) plane, where $\mu > m_N$, i.e. $E > \sqrt{m_N^2 + p^2}$, is confined by the onshell curve, the E axis and the condition $E \leq E_F$ and is therefore only a small fraction of the whole area $E \leq E_F$.

In addition, the nucleons undergo collisions in the course of the FSI. This also gives rise to a finite width for nucleons with energies above the Fermi energy. These widths are determined by evaluating the collision rates for the reactions involving nucleon as incoming particles for energies above the Fermi energy (at $T = 0$ the widths vanish otherwise due to Pauli blocking). For elastic nucleon-nucleon scattering $N + N_2 \rightarrow N_3 + N_4$ e.g. we obtain [16]

$$\Gamma = g \int \frac{d^3 p_2}{(2\pi)^3} d\mu_2 d\mu_3 d\mu_4 d\Omega v_{\text{rel}} \frac{d\sigma_{\text{c.m.}}}{d\Omega} \mathcal{A}_2 f_2 \mathcal{A}_3 (1 - f_3) \mathcal{A}_4 (1 - f_4) \quad (1)$$

where v_{rel} is the relative velocity of the incoming particles and g is the spin-isospin degeneracy factor. The spectral function \mathcal{A} is given by [17]

$$\mathcal{A}_N(\mu_N, p_N, \rho) = \frac{2}{\pi} \frac{\mu_N^2 \Gamma(p_N, \rho)}{(\mu_N^2 - m_N^2)^2 + \mu_N^2 \Gamma^2(p_N, \rho)}. \quad (2)$$

The widths for the FSI reactions are therefore calculated on the same footing as for the groundstate correlations. For other collisional processes, equivalent expressions can be written down. Note that the cross section for the nucleon reactions enters Eq. (1). Since we make use of vacuum cross sections [17], we only calculate the nucleon spectral function for the FSI on the nucleon mass shell. Therefore, the resulting width only depends on density and momentum, but not independently on the nucleon energy. For the nucleons, the total width is obtained by calculating the collision rates for the processes $NN \rightarrow NN$, $NN \rightarrow NR$, $NN \rightarrow \Delta\Delta$ and $NN \rightarrow NN\pi$, which are explicitly implemented in our transport model (for details see Ref. [16]). Other contributions can be neglected, because the multiplicities of the nucleon scattering partners are negligible. For larger energies, when more inelastic multi-particle channels open, we use in Eq. (1) the parametrization for the total cross section from [9] and evaluate the collision width by omitting the Pauli blocking factors for the outgoing fermions. In Fig. 2 we compare the width in the nuclear matter rest frame for density ρ_0 as a function of energy with the onshell widths obtained from the many-body results of [2, 18]. In the considered energy range, the agreement is very good.

We have calculated the nucleon width as a function of momentum. In Fig. 3 the width in the rest frame of the nucleon is shown for different density values as a function of momentum. The width exhibits the zero at the Fermi momentum and then increases with growing inelasticity. The connection of the width in the nucleon rest frame (RF) to that in the nuclear matter rest frame (LAB) is given by

$$\Gamma_{\text{RF}} = \frac{E}{\mu} \cdot \Gamma_{\text{LAB}}.$$

Therefore, Γ_{RF} is larger than Γ_{LAB} .

It should be mentioned that the nucleon width arising from the FSI in Eq. (1) for nucleon energies above the Fermi energy E_F is calculated on the same footing as the width arising from the groundstate correlations in [4, 5] for energies below E_F . The difference is, that in [4, 5] we used an averaged in-medium matrix element, whereas in Eq. (1) the matrix element is substituted by the NN-vacuum cross section. Both widths, however, approach each other because they vanish at $E = E_F$.

III. $S_{11}(1535)$ DECAY WIDTH IN MEDIUM

In this Section we discuss how the nucleon spectral function influences the in-medium decay of nucleon resonances. The strength of the effect is determined by the nucleon width. As discussed in Sec. II, this depends on the momentum of the nucleons stemming from the resonance decay, and the density. There it was shown (see Fig. 3) that with increasing momentum, the in-medium width of the nucleon reaches values comparable to the rho width in vacuum (250 MeV). Therefore, an appreciable effect of nuclear collisional broadening should also be seen. The question remains in which reactions resonances with such large momenta can be prepared. Recently we have discussed η photo- and

electroproduction on nuclei [13, 14] in the onshell limit for the nucleons. In this case, the $S_{11}(1535)$ is the dominating degree of freedom for eta production. Most detected etas stem from the decay of a S_{11} produced in the elementary reaction γN or $\gamma^* N$. The resonance momentum depends on the momentum transfer in this reaction. For virtual photons, the virtuality Q^2 can be chosen independently from the photon energy, which allows for a preparation of resonances with a certain fixed mass and different momenta: In photoproduction, a S_{11} resonance with pole mass has a momentum of 0.78 GeV, in electroproduction at $Q^2 = 3.6$ GeV² a momentum of 3.3 GeV. Also resonances experience a collisional broadening [16]. For resonance momenta up to 1 GeV as encountered in photoproduction, the collision width is rather small (~ 30 MeV at ρ_0) [13]. The calculation for larger resonance momenta of several GeV by using collision rates is difficult because the cross section $NS_{11} \rightarrow X$ in this kinematical regime is unknown. Also estimates based on the total NN cross section would not help because a broadening and/or suppression of the electron-nucleus cross section caused by the collision width depends on a reliable separation of Γ_{coll} into contributions arising from absorptive reactions and processes with a S_{11} or other particles leading to η production in the final state [19]. We therefore focus only on the modification of the in-medium decay width. Since we are interested in η production, we confine our considerations to a modification of the $S_{11}(1535)$ only. Moreover, only the most important decay channels, $N\pi$ and $N\eta$, will be modified. The vacuum resonance widths used in our BUU transport model are parametrized in the same way as in [17, 20], which for the resonance decay $R \rightarrow Nm$ is given by:

$$\Gamma_{R \rightarrow Nm}(\mu_R) = \Gamma_0 \frac{\rho_{Nm}(\mu_R)}{\rho_{Nm}(M_R)}, \quad (3)$$

where Γ_0 denotes the total decay width at the pole mass M_R . In the vacuum, the ρ -function for a decay into a stable nucleon and a stable meson reads:

$$\rho_{R \rightarrow Nm}(\mu) = \frac{p_{Nm}(\mu_R)}{\mu_R} B_l^2(p_{Nm}). \quad (4)$$

Here p_{Nm} is the c.m. momentum of the decay products, μ_R is the resonance mass and B_l is the Blatt-Weisskopf function for the relative angular momentum l of the decay products, which for low c.m. momenta behaves like $\propto p_{Nm}^l$, thereby ensuring the correct momentum dependence of the width close to threshold [20]. In the case of the $S_{11}(1535)$ we have $B_l = 1$. The expression for ρ_{Nm} is close to the general expression for the width $d\Gamma \sim |\mathcal{M}|^2/\mu_R d\Phi_2$ [9]. The factor p_{Nm}/μ_R can be identified with the two-body phase space. The number $\rho_{Nm}(M_R)$ in the denominator in Eq. (3) therefore is part of the matrix element which describes the coupling $R \rightarrow Nm$ and will be left untouched when we go to the medium. For the decay of a resonance into a stable meson and a broad nucleon in the medium, the function ρ_{Nm} in the numerator of Eq. (3) is extended by performing an integration over the nucleon spectral function. This is actually the same as what is done in [20] for the parametrization of the resonance decay in vacuum into a stable nucleon and an unstable meson, e.g. $R \rightarrow N\rho$. Hence, we end up with the expression

$$\Gamma_{S_{11} \rightarrow Nm}^*(\mu_R, p_R, \rho) = \frac{\Gamma_0}{\rho_{Nm}^0} \int_{\mu_N^{\min}}^{\mu_R - m_m} d\mu_N \mathcal{A}_N(\mu_N, p_N, \rho) \frac{p_{Nm}}{\mu_R} \quad (5)$$

with

$$\rho_{Nm}^0 = \frac{p_{Nm}(M_R)}{M_R}.$$

The spectral function $\mathcal{A}_N(\mu_N, p_N, \rho)$ (see Eq. (2) contains the nucleon width $\Gamma(p_N, \rho)$ in the nucleon rest frame (cf. Sec. II) as a function of the lab frame momentum p_N and the density. The dependence of Eq. (5) on p_R arises from the necessity of boosting the nucleon momentum from the c.m. frame into the lab frame. The quantity μ_N^{\min} is a numerical parameter for the minimal nucleon mass considered in our calculations (see Sec. V). It is chosen in a way that the dependence of the widths on this parameter is negligible.

For lower resonance momenta, Pauli blocking of outgoing nucleons is important. This can be accounted for by averaging over the decay angle in the c.m. frame [16]:

$$\tilde{\Gamma}_{S_{11} \rightarrow Nm}^*(\mu_R, p_R, \rho) = \frac{1}{2} \int_{-1}^1 d\cos\theta \Theta(E - E_F(\rho)) \Gamma_{Nm}^*(\mu_R, p_R, \rho).$$

Here, E is the energy of the decaying nucleon and E_F is the local Fermi energy; in the case of offshell nucleons at $T = 0$ the relevant information about the occupation of states in the (local) nuclear matter is given by the Fermi energy and not by the Fermi momentum.

In Fig. 4 we show the results of the decay widths $S_{11} \rightarrow N\eta$ (left panel) and $S_{11} \rightarrow N\pi$ (right panel) for density ρ_0 and different resonance momenta as a function of μ_R . Pauli blocking is not included. The short-dotted curves show the vacuum widths. For the sake of a better resolution in the threshold region, the results are also shown in log plots in the lower part of Fig. 4. The influence of the nucleon spectral function leads to a decrease of the partial widths for larger resonance masses and to finite, non-zero values for masses below the vacuum threshold. This behavior is the more pronounced the larger the resonance momentum is chosen and is strongly connected to the increase of the nucleon width with nucleon momentum observed in Sec. II. However, we have checked that the sensitivity to the components of the nucleon spectral function with very large widths is rather small. Actually, for resonance momenta below 4 GeV we would obtain almost the same results, when we cut the nucleon width at $p_N = 2$ GeV in Fig. 3, leaving the nucleon width constant for momenta above. This is due to the fact that the average nucleon momenta stemming from the S_{11} decay for such resonance momenta does not exceed $p_N \sim 2$ GeV significantly in the given resonance mass range.

Since we want to calculate production reactions of the type $\gamma N \rightarrow S_{11} \rightarrow N\eta$, it is worthwhile to see how the branching ratios $\Gamma_{S_{11} \rightarrow N\eta, \pi} / \Gamma_{\text{tot}}$ are influenced. In Fig. 5 we show the branching ratios for $N\pi$ and $N\eta$ for different momenta as a function of the resonance mass. Since in photon-nucleus reactions also densities smaller than ρ_0 are encountered, we also show the situation for density $\rho = 0.4\rho_0$ on the right-hand side. The short-dotted curves again show the vacuum case. In the $N\pi$ channel we observe a step-like function that comes about because for $m_N + m_\pi < \mu_R < \mu_N + m_\pi$ pion decay is the only relevant decay channel. The partial pion width exhibits a strong smoothening of the step-like structure with p_R which is less pronounced at lower density and/or lower momentum values. The branching ratio $N\eta$ which has a clear cut in the vacuum at the onshell $N\eta$ threshold $m_N + m_\eta$. This step becomes washed out when the density and the resonance momentum increase, whereas the peak structure close to the S_{11} resonance maximum is slightly suppressed.

IV. THE ELEMENTARY REACTION

A. Kinematical situation

We now discuss the sensitivity of photon- and electron-induced reactions to the correlated part of the nucleon spectral function in the groundstate of the nucleus. In [13, 14] we have modeled photon-nucleus and electron-nucleus reactions by the absorption of the real or virtual photon on a single nucleon. Therefore, the quantity of interest is the invariant mass of the photon-nucleon pairs inside the nucleus.

The invariant mass spectra are generated by distributing the nucleons inside the nucleus according to a Woods-Saxon density in coordinate space. Using local density approximation, the momenta and masses are determined according to the spectral function discussed in Sec. II. This is the same procedure also used for the initialization of the nuclei for our transport calculations, for details we therefore refer to [17, 21]. For simplicity, the mean-field potential is neglected. The nucleons satisfy the condition $E_N \leq E_F(\rho)$. Masses and momenta are independent; the maximal possible momentum of a nucleon with mass μ is given by $p_{\max}^2 = E_F^2 - \mu^2$. For $\mu < m_N$ this value is larger than the local Fermi momentum $p_F = \sqrt{E_F^2 - m_N^2}$, and according to Sec. II this is the case for most of the nucleons off the mass shell.

In Fig. 6 we show the invariant mass spectra for a real photon of energy $E_\gamma = 0.8$ GeV and a virtual photon with $Q^2 = 3.6$ GeV 2 and $E_\gamma = 2.71$ GeV. Both kinematics correspond to the second resonance region; the maxima of both distributions (generated e.g. by onshell nucleons at rest) are located at the same value of $\sqrt{s} \sim 1.54$ GeV. The solid spectra show the result using onshell nucleons and are limited in both cases at some maximal and minimal value of \sqrt{s} . It is also seen that the spectrum for virtual photons extends over a much larger c.m. energy range than in the real photon case. This effect is due to Fermi motion [14, 21]. Using the nucleon spectral function, some strength is moved to smaller and also to larger invariant masses, which is accompanied by a depletion in the region of the distribution maximum due to the depletion of the onshell peak.

For the virtual photon case the contribution at low invariant masses extends to \sqrt{s} values smaller than 1 GeV and is not shown here. It is obvious that the contribution for \sqrt{s} values larger than the maximal onshell c.m. energy is more pronounced at finite Q^2 . Indeed, this behavior is the stronger the larger Q^2 becomes. This can be seen as follows. A measure of the strength of this effect is the difference between the maximal c.m. energy values in the onshell and the offshell calculation $\Delta s := s_{\max}^{\text{off}} - s_{\max}^{\text{on}}$. As described above, real and virtual photons probe the same kinematical region if the c.m. energies corresponding to the maximum of the distributions, e.g. for a onshell nucleon at rest, are identical:

$$m_N^2 + 2E_\gamma m_N \stackrel{!}{=} m_N^2 - Q^2 + 2E'_\gamma m_N$$

with momenta pointing into a direction opposite to that of the photon momentum. Therefore, $E_\gamma < E'_\gamma$ and hence $p_\gamma = E_\gamma < p'_\gamma = \sqrt{Q^2 + E'^2}$. The maximal c.m. energies in the onshell spectra are due to nucleons of maximal momentum (i.e. Fermi momentum p_F) with momentum vectors pointing in the opposite direction as the photon momentum vector. Therefore,

$$\begin{aligned}s_{\max}^{\text{on}}(Q^2 = 0) &= m_N^2 + 2(E_\gamma E_F + E_\gamma p_F) \\ s_{\max}^{\text{on}}(Q^2) &= m_N^2 - Q^2 + 2(E'_\gamma E_F + p'_\gamma p_F).\end{aligned}$$

In the offshell spectra, maximal c.m. energies originate from nucleons of some mass $\mu < m_N$ and maximal possible momentum $p_{\max} = \sqrt{E_F^2 - \mu^2} > p_F$. Here we have

$$\begin{aligned}s_{\max}^{\text{off}}(Q^2 = 0) &= \mu^2 + 2(E_\gamma E_F + E_\gamma p_{\max}) \\ s_{\max}^{\text{off}}(Q^2) &= \mu^2 - Q^2 + 2(E'_\gamma E_F + p'_\gamma p_{\max}).\end{aligned}$$

We now construct the differences

$$\begin{aligned}\Delta s(Q^2 = 0) &= \mu^2 - m_N^2 + 2E_\gamma(p_{\max} - p_F) \\ \Delta s(Q^2) &= \mu^2 - m_N^2 + 2\sqrt{Q^2 + E'^2}(p_{\max} - p_F).\end{aligned}$$

Since $E'_\gamma > E_\gamma$, the effect is large when Q^2 becomes large. It should be mentioned, that this also happens for real photons with larger energy.

Due to the behavior of the c.m. spectrum, we can expect an influence of the groundstate correlations on the threshold region of cross sections for particle production. Moreover, close to the maximum of the cross section (i.e. in resonant production processes), a decrease will be observed due to the depletion of strength close to the maximum of the \sqrt{s} spectrum. Eta photo- and electroproduction therefore might be a candidate to observe such effects, because this reaction is dominated by the resonance $S_{11}(1535)$.

B. Cross sections

We now describe how the cross section for the reactions $\gamma A \rightarrow \eta X$ and $eA \rightarrow e'\eta X$ is calculated. For details we refer again to [13, 14], where these reactions were discussed in detail. For the elementary reactions γN and $\gamma^* N$ the outgoing states $P_{33}(1232)$, $D_{13}(1520)$, $S_{11}(1535)$, $F_{15}(1680)$, $N\pi$ and $N\pi\pi$ are important; the cross sections for these processes were discussed there both for $Q^2 = 0$ and 3.6 GeV 2 . It was also mentioned that for η production on nuclei the elementary reaction $\gamma N \rightarrow S_{11}(1535)$ with a subsequent decay into $N\eta$ is the most important source in the second resonance region. At finite Q^2 , this dominance is somewhat reduced due to contributions from secondary processes in the FSI, e.g. $\gamma N \rightarrow N\pi, \pi N \rightarrow S_{11} \rightarrow N\eta$, which in photoproduction are kinematically suppressed. In vacuum, η photoproduction data on the proton are described by the Breit-Wigner ansatz:

$$\begin{aligned}\sigma_{\gamma N \rightarrow S_{11} \rightarrow \eta N}(\sqrt{s}) &= \left(\frac{k_0}{k}\right)^2 \frac{s\Gamma_\gamma(\sqrt{s})\Gamma_{S_{11} \rightarrow X}(\sqrt{s})}{(s - M_{S_{11}}^2)^2 + s\Gamma_{S_{11} \rightarrow X}^2(\sqrt{s})} \frac{2m_N}{M_{S_{11}}\Gamma_0} |A_{1/2}^p|^2, \\ &= \sigma_{\gamma N \rightarrow S_{11}} \cdot \frac{\Gamma_{S_{11} \rightarrow \eta N}(\sqrt{s})}{\Gamma_{S_{11} \rightarrow X}(\sqrt{s})}.\end{aligned}\quad (6)$$

with $\Gamma_\gamma = \Gamma_0 \cdot k/k_0$ and the pole-mass decay width $\Gamma_0 = 0.151$ GeV. The c.m. momentum k of the γp pair depends on the c.m. energy \sqrt{s} (i.e. mass of the resonance), $k_0 = k(M_{S_{11}})$ is the c.m. momentum taken at the pole mass of the S_{11} . This expression can also be used for electroproduction; in the one-photon exchange approximation this is then the cross section for the reaction of the exchanged virtual photon with the nucleon. The cross section for the whole electron nucleon reaction is obtained by multiplication with the virtual photon flux factor Γ_v (Hand convention [22]):

$$\frac{d\sigma_{eN \rightarrow e'N\eta}}{dE'd\Omega} = \Gamma_v \cdot \sigma_{\gamma^* N \rightarrow N\eta} \quad \Gamma_v = \frac{\alpha}{2\pi^2} \frac{s - m_N^2}{2m_N} \frac{E'}{Q^2 E} \frac{1}{1 - \varepsilon}. \quad (7)$$

In Eq. (6), $A_{1/2}$ denotes the transverse helicity amplitude of the S_{11} , which depends on Q^2 . In electroproduction, there is also a longitudinal contribution, which is negligible as well as the dependence of the cross section (7) on the polarization parameter ε [14]. Background processes for both reactions are negligible [23].

The cross section in Eq. (6) is a function of the invariant mass of the photon-nucleon pair (i.e. the resonance mass). Therefore, there will be an influence of the groundstate correlations as described in the last section. Moreover, the decay widths of the $S_{11}(1535)$ enter the expression as well as the branching ratio for $N\eta$. In the onshell case, the cross section (6) has a cut at the $N\eta$ vacuum threshold $\sqrt{s} = m_N + m_\eta$ due to the branching ratio (cf. Fig. 5). This is different when the modified branching ratio is used: The mass spectra of the $S_{11}(1535)$ resulting from the elementary reaction, are essentially given by the c.m. energy spectra in Fig. 6. Since the modified branching ratio assumes finite values at invariant masses below $m_N + m_\eta$, all resonances with such small masses will yield small but finite contributions to η production in nuclei. This will clearly have an impact on the final result. This effect will be more pronounced at finite Q^2 , because here the sensitivity to the correlated part of the nucleon spectral function is larger and due to the large resonance momenta also the modification of the branching ratio will be stronger.

We now show how the cross section for the $\gamma A \rightarrow \eta X$ reaction is calculated within our model [16, 24]:

$$\sigma_{\gamma A \rightarrow \eta X}(E_\gamma) = g \int_V d^3r \int \frac{d^3p_N}{(2\pi)^3} d\mu_N \mathcal{A}(\mu_N, p_N, \rho) \Theta(E_F(\rho(\vec{r})) - E_N) \sum_f \sigma_{\gamma N \rightarrow f} M_f^\eta, \quad (8)$$

where the coordinate space integral extends over the nuclear volume and the sum runs over all possible final states of the elementary reaction listed above. M_f^η are multiplicity factors taking into account how many etas were produced by the particles contained in the final state f . For the energies under consideration, M_f^η usually equals one or zero. The multiplicity factor includes the effects from the FSI and will be determined by the BUU model, described in Sec. V. For η electroproduction, a formula analogous to Eq. (8) exists for the calculation of the cross section $d\sigma(eA \rightarrow e'\eta X)/(d\Omega dE')$. The main difference is that the elementary cross sections $\sigma_{\gamma N}$ have to be substituted by their counterparts for the electron-nucleon reaction, $d\sigma_{eN}/(dE' d\Omega)$. More details can be found in [14, 21].

V. THE BUU MODEL

For the description of the FSI we make use of the BUU transport model developed in [17, 21, 25], which yields a realistic description of different reaction types included in the FSI as elastic and inelastic collisions, resonance formation and decay and particle production by string fragmentation in high energy events. The model is based upon the BUU equation, which describes the offshell space-time evolution of the spectral phase space density $F_i = \mathcal{A}_i f_i$ of all particle species $i = N, \pi, \eta, P_{33}, S_{11}, \dots$:

$$\left(\frac{\partial}{\partial t} + \vec{\nabla}_p H_i \cdot \vec{\nabla}_r - \vec{\nabla}_r H_i \cdot \vec{\nabla}_p \right) F_i(\vec{r}, \vec{p}, \mu; t) = I_{\text{coll}}[F_N, F_\eta, F_{S_{11}}, \dots]. \quad (9)$$

Here \mathcal{A}_i is the spectral function and H is a relativistic Hamilton function

$$H_i = \sqrt{(m_i + S_i)^2 + p^2}. \quad (10)$$

In the case of baryons, H includes an effective scalar mean-field potential S_i . For the present calculations, we use the same momentum dependent parametrization as in [13]. The reaction processes in the FSI are described by a set of BUU equations in the following way: Whereas the propagation according to the Hamilton function is described by the left-hand side, the right-hand side (collision integral) includes a loss and a gain term, consisting of collision rates for the different collision processes and accounting for the gain and the loss of the spectral phase space density F_i at each point caused by the collisions. The BUU equations are therefore coupled via the collision terms. Pauli blocking is explicitly taken into account in each collision reaction with outgoing nucleons. Therefore, the S_{11} widths without Pauli blocking have to be used when determining whether a resonance decays or not in order to avoid double counting.

The common method to solve this system of equations is the so-called test particle ansatz. The spectral phase space density F_i is substituted by

$$F_i(\vec{r}, \vec{p}, \mu; t) \propto \sum_i \delta(\vec{r} - \vec{r}_i(t)) \delta(\vec{p} - \vec{p}_i(t)) \delta(\mu - \mu_i(t)). \quad (11)$$

In the absence of collisions (i.e. vanishing collision integral), the BUU equation is fulfilled by this ansatz if the test particles obey certain equations of motion. In the onshell approximation, these are the Hamiltonian equations of motion:

$$\dot{\vec{r}} = \frac{\partial H}{\partial \vec{p}}, \quad \dot{\vec{p}} = -\frac{\partial H}{\partial \vec{r}}.$$

For the offshell propagation of the nucleons, we use the method developed in [10]. There a scalar 'offshell potential' was introduced by

$$\Delta\mu(t) = (\mu_N(t_{\text{cr}}) - m_N) \frac{\rho(t)}{\rho(t_{\text{cr}})}$$

with the baryon density ρ and the creation time t_{cr} . The full Hamilton function for the nucleons then reads

$$H = \sqrt{(m_N + U_S + \Delta\mu)^2 + p^2}.$$

This ansatz ensures that the offshellness vanishes when the nucleon test particles travel into the vacuum. For the propagation, the usual equations of motion are used with the Hamilton function including the offshell potential. The time evolution of the offshell mass is directly given by

$$\mu_N(t) = m_N + \Delta\mu(t) = m_N + (\mu_N(t_{\text{cr}}) - m_N) \frac{\rho(t)}{\rho(t_{\text{cr}})},$$

which means that the nucleon mass is shifted towards the pole mass m_N when travelling to regions of small density. This equation of motion does not prevent the mass from becoming negative during the propagation. In order to avoid such effects, we choose a minimal nucleon mass $\mu_N^{\text{min}} = 0.4$ GeV in the initialization and collisions. We have checked that this value has no influence on the final results. For consistency, we use this value also in the calculation of the modified S_{11} decay width in Eq. (5).

This set of equations has found its a posteriori justification in recent work in which test particle equations of motion were derived from the Kadanoff-Baym equation using a gradient expansion [11, 12]. The equations derived there become equal to the ones used here in the limit of not too large offshellness and $\Gamma \sim \rho$.

VI. RESULTS

In Fig. 7 we show the cross section for the reaction $\gamma\text{Ca} \rightarrow \eta X$, determined according to Eq. (8). The solid curve shows the result with onshell nucleons. The dotted line is the offshell result but using vacuum widths for the elementary cross sections involving the S_{11} (Eq. (6)). We see that the curve is lowered compared to the onshell calculation, especially in the region close to the maximum. This is essentially the effect of the groundstate correlations and originates in the depletion in the c.m. energy spectra close to the maxima, as discussed in Sec. IV A. Moreover, no effects in the region close to threshold are observed, as anticipated before. Since the the absolute threshold for (coherent) η production on nuclei is located at $E_\gamma \sim 0.55$ GeV, there are no contributions below the onshell threshold. The dashed curve finally shows the result including both the nucleon spectral function and the modified decay widths for the S_{11} . Compared to the dotted offshell curve, an increase in the energy region from threshold to the maximum can be seen. This is the effect of the width modification. However, the net increase (i.e. compared to the onshell result) for energies larger than 0.8 GeV is essentially zero, because the increase caused by the modified widths is canceled by the decrease due to the groundstate correlations. Therefore, we are left only with a slight increase in the threshold region with respect to the onshell calculation, yielding a closer agreement with the experimental data from [26].

We now turn to η electroproduction. Here we expect a somewhat larger effect: On the one hand, the virtual photon is more sensitive to the large momentum component of the spectral function of correlated nucleons in the elementary reaction. On the other hand, the S_{11} are produced with larger momenta, which increases the medium effect of the decay widths. In Fig. 8 we show several scenarios for the reaction $e\text{Ca} \rightarrow e'\eta X$. The lower plot shows the threshold region in more detail. The solid and dash-dotted curves show the onshell results with and without FSI. It is seen that the calculation with FSI yields a somewhat larger cross section. This effect, discussed in [14], is due to the fact that in reactions with large momentum transfer a large contribution of etas is produced in secondary processes in the FSI. Therefore, the absorption of etas from the primary production chain $\gamma N \rightarrow S_{11} \rightarrow \eta N$ is balanced. For small photon energies $E_\gamma < 2.3$ GeV this is even more obvious. Due to the secondary contributions, which are not present in a calculation without FSI, the threshold is lowered down to energies of about 1.8 GeV. It should be mentioned, that the absolute (coherent) threshold for this reaction is given by $E_\gamma = m_\eta^2 + (m_\eta^2 + Q^2)/(2m_A) \sim 0.6$ GeV is located at much smaller photon energies. The dashed and dotted lines present the offshell calculation with and without FSI, including the modified S_{11} decay widths. The calculation without FSI is enhanced compared to the onshell result by up to $\sim 20\%$ close to the maximum of the curve. Similar to photoproduction, this increase is due to the width modification. As mentioned in Sec. IV B, also resonances with masses below the free $N\eta$ threshold contribute now, this effect is stronger for large Q^2 . Moreover, there is a strong subthreshold effect caused by the groundstate correlations. In

the full calculation with FSI, the difference to the onshell counterpart becomes somewhat smaller. This is mainly due to the contribution of secondary processes at higher energies (yielding approximately one half of all etas [14]), which are essentially identical for the onshell and the offshell case. However, the remaining increase is larger than in photoproduction. In the threshold region, the curves with and without FSI are close to each other, because there only etas from the primary reaction influenced by the groundstate correlations contribute. The difference to the solid onshell curve, however, is smaller than in the scenario without FSI, because the onshell threshold is strongly lowered by the FSI.

VII. SUMMARY

We have calculated η photo- and electroproduction on nuclei within the BUU transport model. In contrast to [13, 14], we take into account that the nucleons are correlated in the nuclear groundstate and acquire a finite width due to collision reactions during the FSI. This has an influence on the kinematics of the elementary photon-nucleon reaction. Furthermore, we have discussed how the possibility of a resonance decay into broad nucleons might modify the in-medium decay width of the $S_{11}(1535)$. Here we found strong deviations from the vacuum case in particular for large resonance momenta. Combining all these issues together with the model for the offshell propagation developed in [10], we showed that there is indeed an influence on the η production cross section on nuclei, which is more pronounced at large momentum transfer, i.e. in electron induced reactions at large Q^2 . Besides contributions below the threshold of the onshell calculations, an increase of the cross section for energies up to the maximum is observed.

The model presented here is particularly suitable for an investigation of offshell effects on incoherent particle production yields. In particular, it could also be applied to reactions with high energy photons such as J/ψ production on nuclei, where searches for color transparency phenomena have to rely on an accurate description of more involved, but nevertheless interesting effects.

ACKNOWLEDGMENTS

We acknowledge many valuable discussions with M. Post. This work was supported by DFG.

[1] L.P. Kadanoff and G. Baym, *Quantum Statistical Mechanics*, Benjamin, New York, 1962.
 [2] O. Benhar, A. Fabrocini, and S. Fantoni, Nucl. Phys. A **550**, 201 (1992); O. Benhar, A. Fabrocini, and S. Fantoni, Nucl. Phys. A **505**, 267 (1989).
 [3] C. Ciofi degli Atti and S. Simula, Phys. Rev. C **53**, 1689 (1996).
 [4] J. Lehr, M. Effenberger, H. Lenske, S. Leupold, and U. Mosel, Phys. Lett. B **483**, 324 (2000).
 [5] J. Lehr, H. Lenske, S. Leupold, and U. Mosel, Nucl. Phys. A **703**, 393 (2002).
 [6] O. Benhar, A. Fabrocini, S. Fantoni, G.A. Miller, V.R. Pandharipande, and I. Sick, Phys. Rev. C **44**, 2328 (1991).
 [7] A. Sibirtsev, W. Cassing, and U. Mosel, Nucl. Phys. A **679**, 497 (2001).
 [8] A. Sibirtsev, W. Cassing, and U. Mosel, Z. Phys. A **358**, 357 (1997).
 [9] K. Hagiwara *et al.*, Particle Data Group, Phys. Rev. D **66**, 010001 (2002).
 [10] M. Effenberger and U. Mosel, Phys. Rev. C **60**, 051901 (1999).
 [11] W. Cassing and S. Juchem, Nucl. Phys. A **665**, 377 (2000).
 [12] S. Leupold, Nucl. Phys. A **672**, 475 (2000).
 [13] J. Lehr, M. Post, and U. Mosel, Phys. Rev. C (to be published), nucl-th/0306024.
 [14] J. Lehr and U. Mosel, Phys. Rev. C **68** (to be published), nucl-th/0307009.
 [15] S. Stringari, M. Traini, and O. Bohigas, Nucl. Phys. A **516**, 33 (1990).
 [16] M. Effenberger, A. Hombach, S. Teis, and U. Mosel, Nucl. Phys. A **613**, 353 (1997).
 [17] M. Effenberger, E.L. Bratkovskaya, and U. Mosel, Phys. Rev. C **60**, 044614 (1999).
 [18] M. Baldo, I. Bombaci, G. Giansiracusa, U. Lombardo, C. Mahaux, and R. Sartor, Nucl. Phys. A **545**, 741 (1992).
 [19] J. Lehr and U. Mosel, Phys. Rev. C **64**, 042202 (2001).
 [20] D.M. Manley and E.M. Saleski, Phys. Rev. D **45**, 4002 (1992).
 [21] J. Lehr, M. Effenberger, and U. Mosel, Nucl. Phys. A **671**, 503 (2000).
 [22] L.N. Hand, Phys. Rev. **129**, 1834 (1963).
 [23] G. Penner and U. Mosel, Phys. Rev. C **66**, 055212 (2002).
 [24] M. Effenberger, A. Hombach, S. Teis, and U. Mosel, Nucl. Phys. A **614**, 501 (1997).
 [25] S. Teis, W. Cassing, M. Effenberger, A. Hombach, U. Mosel, and G. Wolf, Z. Phys. A **356**, 421 (1997).
 [26] M. Röbig-Landau *et al.*, Phys. Lett. B **373**, 45 (1996).

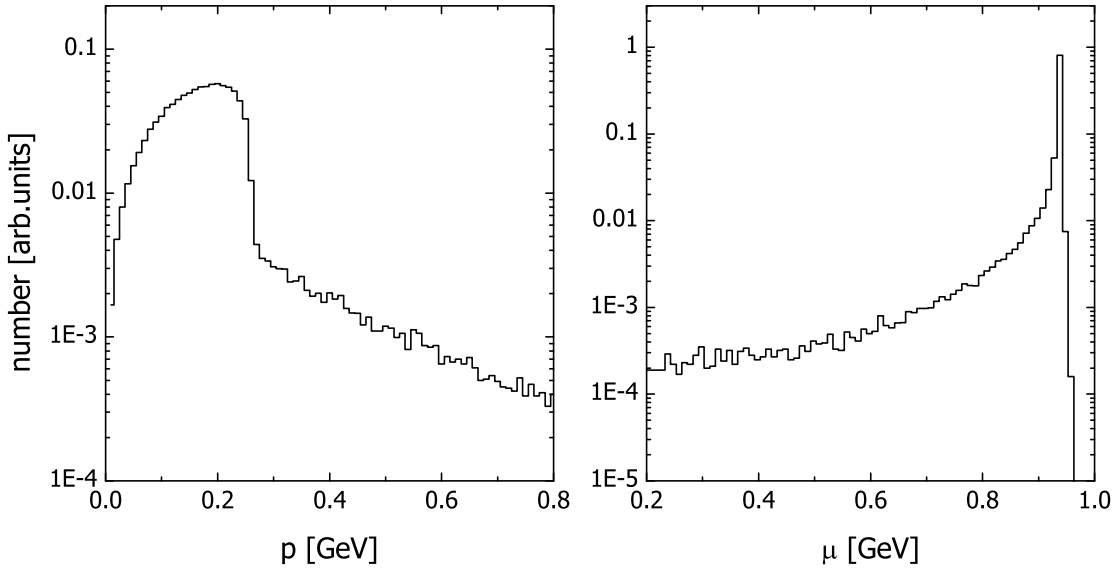


FIG. 1: Momentum and mass spectra for the nucleons inside calcium including groundstate correlations using local density approximation.

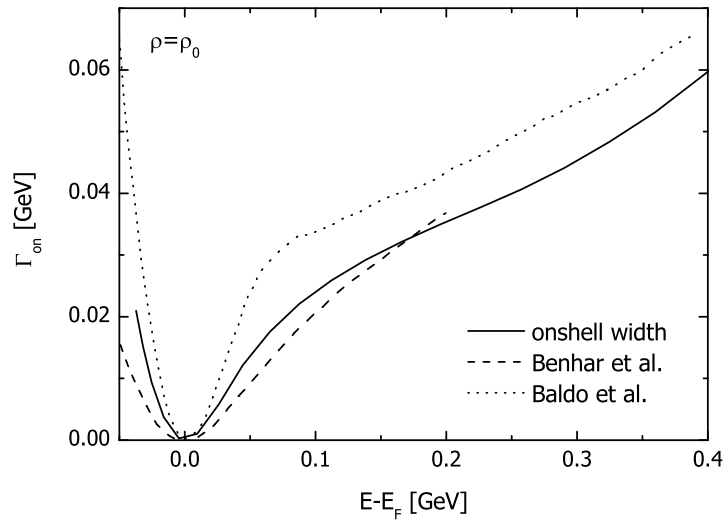


FIG. 2: Onshell width of the nucleons calculated at nuclear matter density ρ_0 as a function of the energy. The dashed and dotted curves show the result from Benhar et al. [2] and Baldo et al. [18].

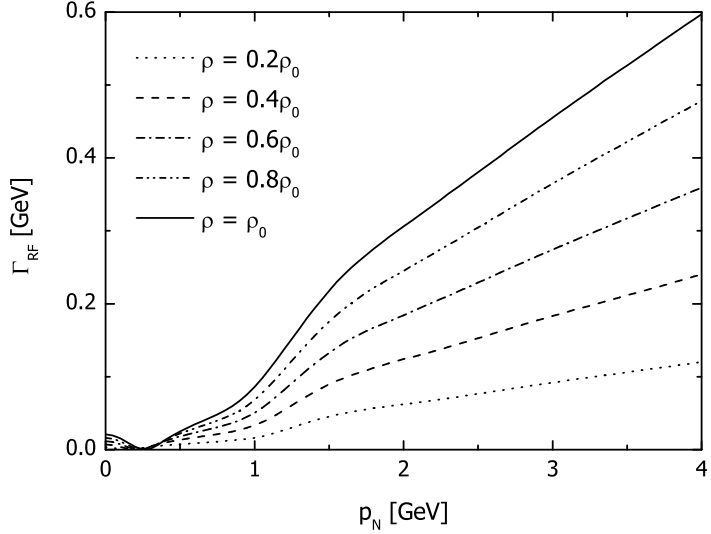


FIG. 3: Onshell nucleon width as a function of the nucleon momentum in the lab frame for different densities, calculated in the rest frame of the nucleon.

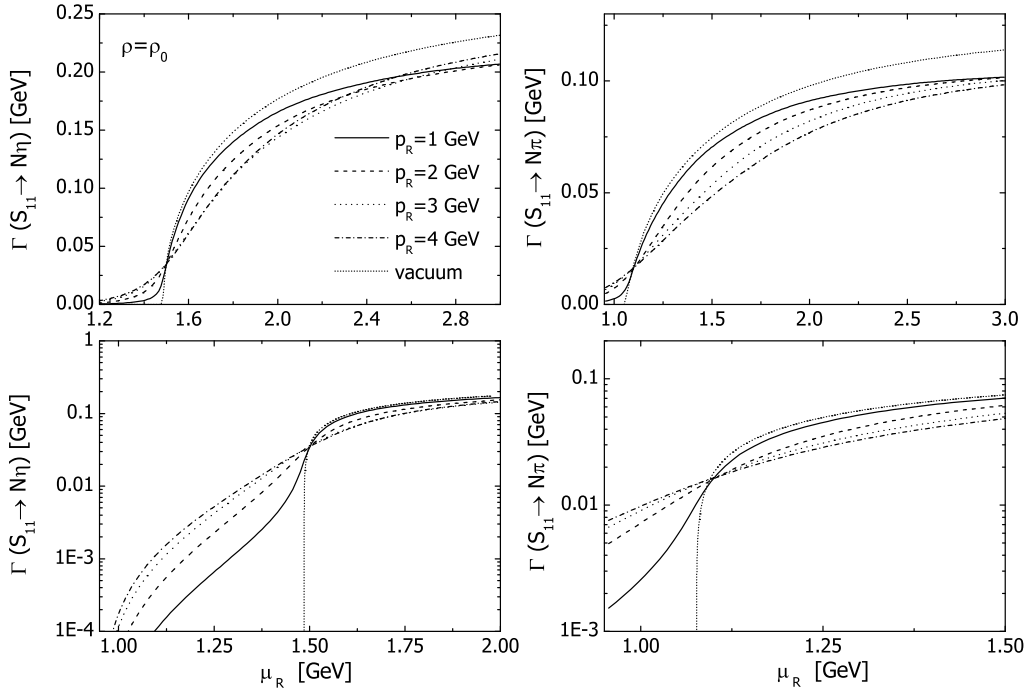


FIG. 4: In-medium decay width of the $S_{11}(1535)$ for the channels $N\eta$ and $N\pi$ as a function of the resonance mass. The different curves correspond to different resonance momenta as indicated in the legend. The short-dotted curves show the vacuum case. The calculations were performed at nuclear matter density ρ_0 . Pauli blocking is not included.

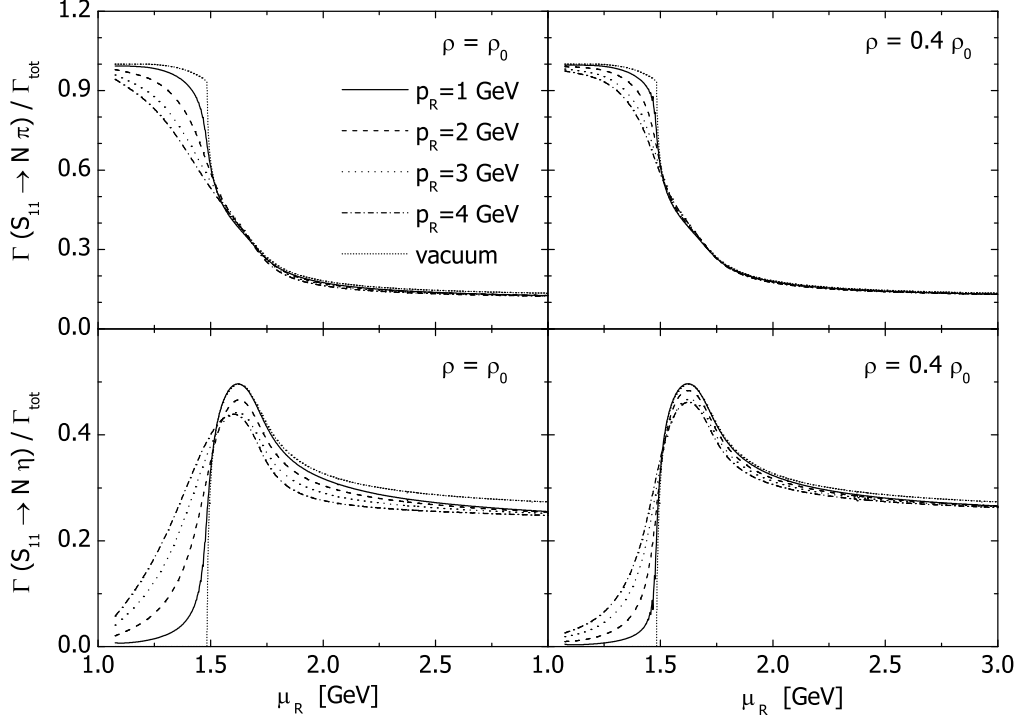


FIG. 5: S_{11} branching ratios for $N\eta$ and $N\pi$, modified with the nucleon spectral function, as a function of the resonance mass. The left panels show the results for density ρ_0 , the right panels for density $0.4\rho_0$. The different curves correspond to different resonance momenta as indicated in the legend, the short-dotted curves show the vacuum case. Pauli blocking is not taken into account.

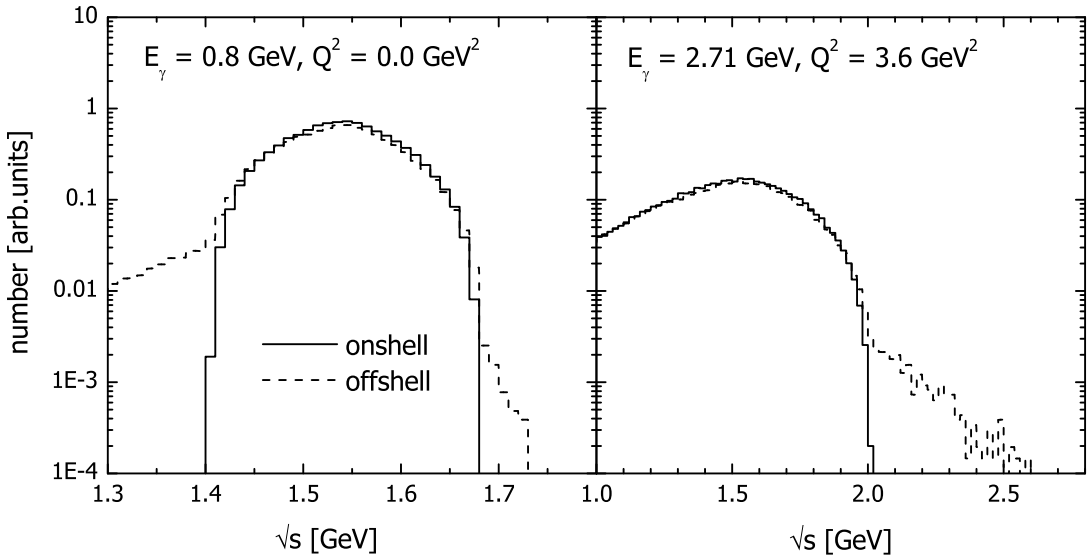


FIG. 6: Invariant mass spectra of photon-nucleon pairs in calcium for real and virtual photons. For both kinematics, the absorption of the photons on an onshell nucleon at rest corresponds to an excitations of a resonance with mass $\mu_R \sim 1.54$ GeV. The solid and dashed curves show results without and with nucleon spectral function due to groundstate correlations.

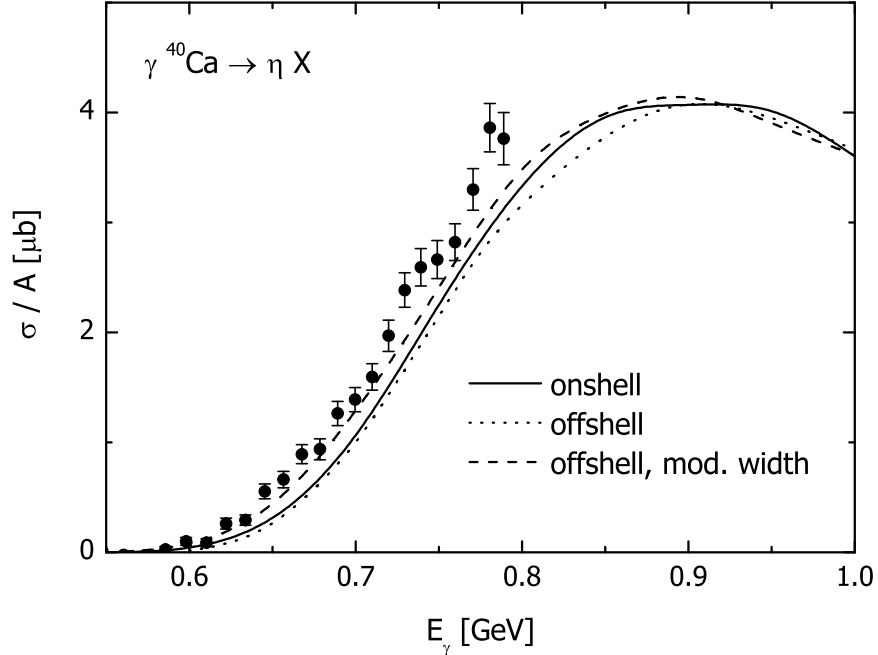


FIG. 7: Results for the reaction $\gamma\text{Ca} \rightarrow \eta X$. The curves correspond to calculations with onshell nucleons (solid), offshell nucleons (dotted) and offshell nucleons with modified S_{11} widths (dashed). The data are from [26].

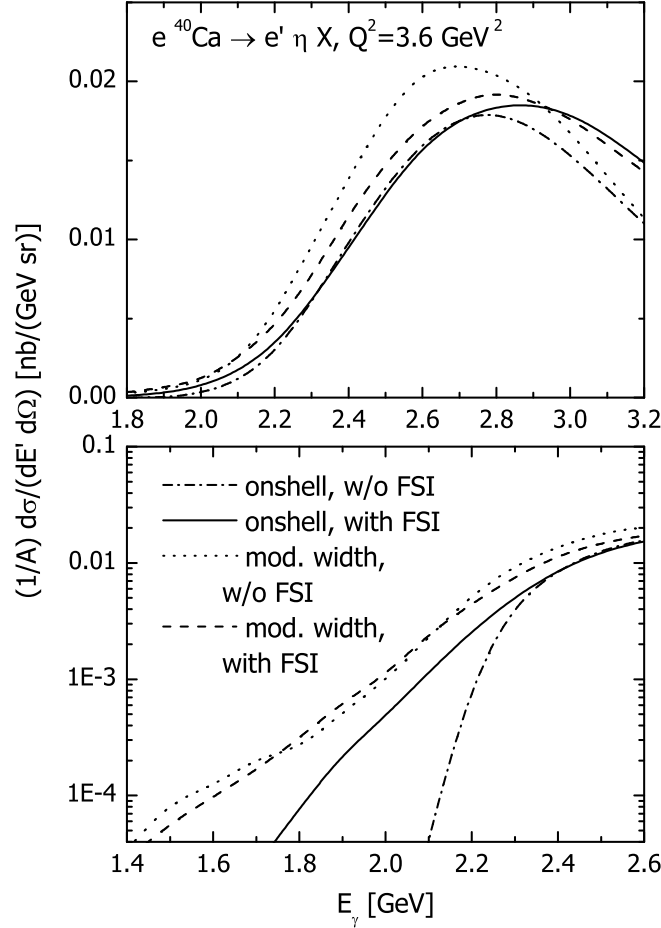


FIG. 8: Cross section for the reaction $e^40\text{Ca} \rightarrow e'\eta X$. The solid and dash-dotted curves show the onshell calculation with and without FSI, the dashed and dotted lines show the results with offshell nucleons and modified S_{11} width, with and without FSI.